JPE 12-4-7

http://dx.doi.org/10.6113/JPE.2012.12.4.578

Grid-Connected Photovoltaic System Based on a Cascaded H-Bridge Inverter

Mohammad-Ali Rezaei*, Hossein Iman-Eini†, and Shahrokh Farhangi*

†*School of Electrical and Computer Engineering, College of Engineering, University of Tehran, Tehran, Iran

Abstract

In this paper a single-phase Cascaded H-Bridge (CHB) inverter for photovoltaic (PV) applications is presented. Based on the presented mathematical analysis, a novel controller is introduced which adjusts the inverter power factor (PF) and manipulates the distribution of the reactive power between the cells to enhance the operating range of the CHB inverter. The adopted control strategy enables tracking of the maximum power point (MPP) of distinct PV strings and allows independent control of the dc-link voltages. The proposed controller also enables the inverter to operate under heavily unbalanced PV conditions. The performance of the CHB inverter and the proposed controllers are evaluated in the PSCAD/EMTDC environment. A seven-level CHB-based grid connected laboratory prototype is also utilized to verify the system performance.

Key words: cascaded H-bridge, multilevel inverter, stability, photovoltaic system

I. INTRODUCTION

Grid-connected PV systems are a popular and well established technology due to their contributions to clean energy generation. The aim of this technology is to extract the maximum possible energy out of PV modules by tracking its MPP, injecting a high-quality current into the grid and enhancing the overall efficiency of the PV system. The relatively high cost of PV modules has led researchers to focus on cheap and innovative inverter topologies to make PV power generation more attractive. This, in turn, has resulted in a high diversity of inverter topologies and system configurations. However, the most common topology for single-phase grid connected systems is the two-level multi-string inverter [1]. In this topology, several dc-dc converters, each of which is connected to a PV array, share a single dc-link as an output. This topology offers several advantages such as: easy expansion of the system power by adding more dc-dc converters and PV modules, independent MPP tracking for each PV array and simple control schemes.

In the past decade, multilevel inverter topologies [2] have been introduced to PV applications [3]. These topologies can inject a high quality current with a low harmonic distortion to the grid, reach higher efficiencies with low switching frequency techniques and eliminate the bulky line-side filter and transformer that are required in the integration of PV systems to a high voltage grid. Besides, multilevel topologies feature several dc-links which can be used to lessen the effects of module mismatches in PV arrays.

Among the different types of multilevel converters, the CHB is the most attractive topology because of its modularity, simple physical layout, smaller number of components, and higher reliability [4,5]. In addition, the necessity of isolated dc sources makes this topology an ideal candidate for PV applications.

Controlling a CHB inverter is a rather simple task when the inverter operates under symmetrical conditions (e.g. when the H-bridge cells transfer an equal amount of power and have the same reference voltage). This however, is not the case in PV applications, since there is the possibility of unequal solar radiations, aging of the PV panels and the connection of different PV panel types to each H-bridge. It has also been reported in the literature that the CHB control system is prone to an intrinsic instability problem which results in a limited operation range for the system [6]. This problem is due to the nature of the control system which has to control $n + 1$ variables (one output current and n dc voltages) through n switching functions. This limited

Manuscript received Jan. 5, 2012; revised May 20, 2012
Recommended for publication by Associate Editor Yong-Sug Suh.
†Corresponding Author: imaneini@ut.ac.ir
Tel: +9821-82084962, Fax: +9821-88778690, University of Tehran
*School of Electrical and Computer Engineering, College of Engineering, University of Tehran, Iran

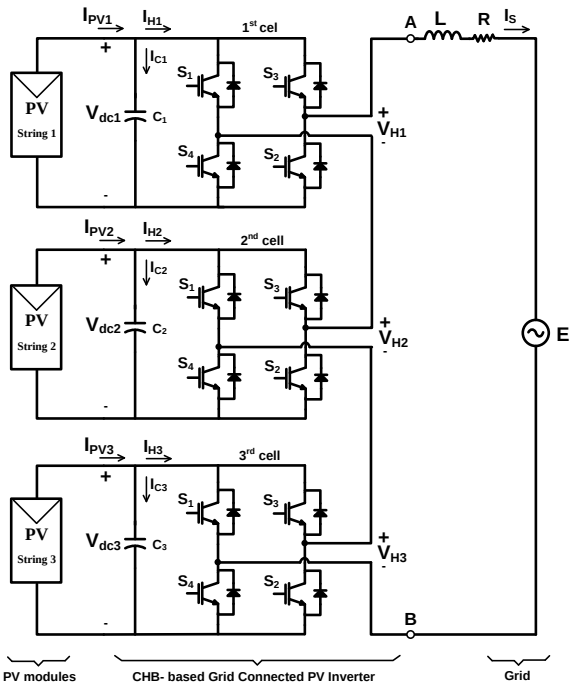

Fig. 1. Schematic representation of seven-level CHB-based grid connected PV inverter.

operation range severely deteriorates the overall reliability of CHB-based grid connected PV systems. Because, in the case of a malfunction or shading of a PV string the whole system shuts down due to instability.

During the past decade, several control methods have been proposed for CHB-based PV systems to fulfill the task of current controlling and MPPT [7]–[10]. However, despite of the aforementioned merits of CHB-based PV systems, they still have some control issues have not been comprehensively analyzed in technical literature.

In [7], a fully fuzzy logic based controller has been presented which allows for the control of CHB inverters without any intermediate controller. Despite its simplicity, since this controller does not use any modulator, it does not exploit the harmonic cancellation opportunity of CHB inverters. Also, the operation constraints of the controller have not been analyzed in this paper. Therefore, it does not provide a viable solution to address the stability issues of CHB inverters.

The presented control scheme in [8] uses the conventional cascade control strategy to regulate the dc voltages and to perform the MPPT task. Despite the successful operation of the controller in balanced PV conditions, it still suffers from the instability problem. Because this approach uses only *n* variables to control the inverter.

A hybrid CHB multilevel inverter with an easy to implement control scheme has been presented in [9]. Reference [10] also presents several grid-connected multilevel inverter topologies for PV applications. Despite the presented simulation results and experimental validations, none of the aforementioned methods discuss the operation criteria of their presented control schemes.

Based on the presented mathematical analysis, this paper presents a novel voltage balancing strategy for CHB inverters. Also, taking the PF of the inverter as a degree of freedom, a novel reactive power controller has been presented that enables the inverter to operate under heavily unbalanced PV conditions.

II. Topology Description

A. Principles of Operation

A single-phase seven-level CHB structure is shown in Fig.1. This structure is coupled with the grid through a filter inductor. The inductor is utilized to program the inverter current to be sinusoidal. The seven-level inverter consists of three series connected H-bridges (or equivalently, cells). Each cell has four power switches with anti-parallel diodes and a dc-bus capacitor. PV strings are connected in parallel to each of these capacitors.

Several switching strategies have been proposed for CHB converters [11]. This paper adopts the Phase-Shifted PWM (PSPWM) switching strategy because it evenly distributes power among each of the cells and it is very easy to implement. For a seven-level CHB inverter, the PS-PWM technique requires six carrier waveforms displaced with $\varphi=2\pi/6$ radians phase-shift in relation to each other.

B. Mathematical Model

To mathematically model the behavior of a CHB inverter, the relationship between the inverter current, the dc voltages and the modulating waveforms should be derived. It should be noticed that the presented analysis is valid for any switching scheme. Hereafter, in this paper, capital letters indicate the RMS of variables, while small letters represent the waveform of variables.

Assuming steady-state operation of the inverter, it is possible to define the modulating waveform of the j^{th} cell as:

$$s_j = \frac{(v_{Hj})_1}{V_{dcj}} \tag{1}$$

where $(v_{Hj})_1$ and V_{dcj} are the fundamental harmonic of the ac-side voltage waveform and dc voltage of the j^{th} cell, respectively. In the steady-state condition, the modulating waveforms are sinusoidal and bounded by the [-1, 1] interval (assuming linear operation of the inverter).

Using the modulating waveforms, the behavior of the system can be fully described by the following set of equations:

$$\frac{di_s}{dt} = \frac{1}{L}(\sum_{k=1}^{3} s_j V_{dcj} - Ri_s - e) \quad (2)$$

$$\frac{dV_{dcj}}{dt} = \frac{1}{C_k}(i_{PVj} - s_j i_s) \quad where \quad j = 1,2,3 \quad (3)$$

where i_s indicates the input current of the inverter, e is the grid voltage and L, R and C_k indicate the inductance and resistance of the filter inductor and the capacitor of the j^{th} cell, respectively. Equation (2) describes the dynamics of the inverter's input current and (3) describes the dynamics of the dc voltages.

To help gain a better insight into the CHB inverter instability problem, this paper uses the phasor theory to analyze the inverter operation. So, applying the phasor theory to (2) yields:

$$\overrightarrow{S_1}V_{dc1} + \overrightarrow{S_2}V_{dc2} + \overrightarrow{S_3}V_{dc3} = E + (j\omega L + R)\overrightarrow{I_s} \quad (4)$$

where E (the grid voltage) is the reference of the phase measurement and $\overrightarrow{S_j}V_{dcj}$ is the ac-side voltage phasor of the j^{th} cell (all in RMS). It can be inferred from (4) that the stable operation of the CHB inverter requires the sum of the dc voltages to be greater than the maximum of the grid voltage.

The overall ac-side voltage phasor of the inverter can also be written as:

$$\vec{V}AB = \sum_{k=1}^{3} \vec{S}kV_{dck} \quad (5)$$

Neglecting the inverter loss, the following equation can be derived for the transferred power from the dc side to the ac side:

$$P_j = V_{dcj}\overline{I_{Hj}} = \vec{V}_{Hj} \cdot \vec{I}_S \quad (6)$$

where P_j is the transferred power from the dc side (or the j^{th} PV string) to the grid, $\overline{I_{Hj}}$ is the dc-side average current of the j^{th} cell, and the (·) symbol indicates the dot product of two vectors. Using (6), the variable $\overline{I_{Hj}}$ can be written as:

$$\overline{I_{Hj}} = I_{PVj} = \frac{\vec{V}_{Hj}}{V_{dcj}} \cdot \vec{I}_S = \vec{S}_j \cdot \vec{I}_S \quad (7)$$

where I_{PVj} is the PV string current (which is a dc term) and is equal to $\overline{I_{Hj}}$ at the steady state. By decomposing the ac-side current phasor into its direct and orthogonal components (the d-q frame) and noting (6) and (7), the following equation is derived for the total transferred power P_{tot} (at steady state):

$$E \cdot I_{sd} = P_{tot} = V_{dc1}I_{PV1} + V_{dc2}I_{PV2} + V_{dc3}I_{PV3} \quad (8)$$

where I_{Sd} indicates the direct component of the inverter phasor current.

III. Stability Analysis

A. Instability Description

The control system for every CHB-based grid connected PV system is composed of the following two main parts:

1) Current controller.

2) Voltage or power balancing controller.

Each part of the control system can contribute to a instability problem. The current controller introduces a phase-delay to the control system variables which may cause instability due to the reduced phase-margin of the system. Since proper tuning of the current controller can prevent this instability, it is not discussed in this paper.

Based on the dc-side current of the inverter, the voltage balancing (or power balancing) controller instability can be described as follows [12]:

For the inverter to operate stably, the cells' dc side average current ($\overline{I_{Hj}}$) should be equal to their associated PV string current (I_{PVj}) at the reference voltage. Therefore, the voltage balancing controller should provide the current balancing conditions by adjusting the modulation index of each cell.

According to (7) and in a specific (PF), if the PV string current of one cell increases, the modulation index of the cell should be increased as well. At some point of operation, where the PV current of a cell becomes comparable to the RMS current of the inverter, a further increase in the PV current will cause the modulation index of the cell to exceed unity and the inverter will become unstable. The same line of reasoning is also valid in case of a reduction in the PV current.

It should be noted, in spite of the fact that the modulating waveform of one cell can increase up to $4/\pi$ in the stable operation region of the inverter, due to increased current THD, in this paper, the criteria for instability is defined as the unity modulation index. However, if non-linear operation of the inverter is tolerable in a specific application, the criteria can be changed to higher values.

B. Mathematical Analysis

The ac-side voltage of the inverter can be divided into two orthogonal components:

1) The Active Power Transferring Component (APTC) which is the projection of $\vec{V}_{AB}$ over the current vector $\vec{I}_s$.

2) The Reactive Power Transferring Component (RPTC) which is orthogonal to the current vector $\vec{I}_S$.

These components can be derived as:

$$(V_{AB})_P = \vec{V}AB \cdot \frac{\vec{I}_S}{I_S} = e \times \cos(\varphi) + RI_S \quad (9)$$

and:

$$(V_{AB})_Q = e \times \sin(\varphi) + \omega LI_s \quad (10)$$

where the *P* and *Q* indices indicate the active and reactive power transferring components respectively, φ is the current angle of the inverter, and I_s is the magnitude of $\vec{I}_S$. It should also be noted that in (9) and (10), the resistor and the inductor voltage terms (RI_S) and (ωLI_s) can be omitted, because they are only a small portion of the ac-side voltage of the inverter.

According to (6), the APTC of each cell is proportional to its dc-side current (I_{Hj}) and as mentioned in Section III-A for the stable operation of the inverter, the condition $\overline{I_{Hj}} = I_{PVj}$ should be satisfied at the steady state. As a result, $(V_{AB})_P$ should be shared between the cells proportional to their dc-side reference current. This produces the active power transferring component of the modulation index ($(m_j)_P$) of the cells, as follows:

$$(m_j)_P = \frac{I_{PVj}}{\sum_{k=1}^{3} I_{PVk}} \frac{\sqrt{2}(V_{AB})_P}{V_{dcj}} \quad (11)$$

The RPTC has no effect on the voltage balancing of the cells. Therefore, it can be distributed between the cells in many ways. Since the proposed control strategies in [7], [9], [10] have no control over the reactive power transfer of the cells, they simply share the RPTC along with the APTC, which means that in (11), $(V_{AB})_P$ can be replaced by V_{AB} to calculate the overall modulation index of each cell (m_j).

For control schemes that use a specific pattern to distribute the reactive power (e.g. the control scheme presented in [6]), or the presented control strategy in this paper, which manipulates the reactive power transfer of each cell, the RPTC of the each cell modulation index can be calculated as:

$$(m_j)_Q = \frac{\sqrt{2}(V_{Hj})_Q}{V_{dcj}} \quad (12)$$

where $(V_{Hj})_Q$ is the RPTC of the j^{th} cell. As a result, the overall modulation index of the j^{th} cell can be calculated as:

$$m_j = \sqrt{(m_j)^2_P + (m_j)^2_Q} \quad (13)$$

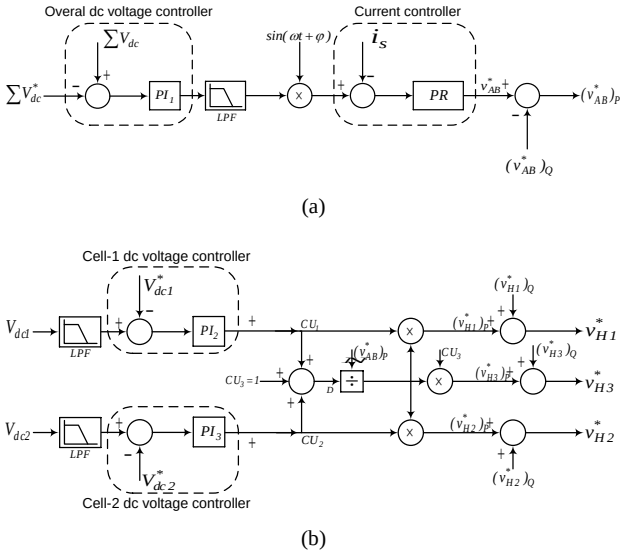

Fig. 2. Configuration of (a) current controller, and (b) dc voltage control subsystems

and the inverter operation is stable if $m_j \le 1$ for each cell. According to (7) and (8), the minimum stable current of the inverter, operating in unity PF, may be achieved if:

1) The modulation index of the cell with highest PV string current is unity.

2) The cell with highest PV string current transfers only active power.

Based on these conditions, and from the active power balancing of the cell at the unity modulation index, the minimum stable current can be deduced as:

$$I_{s\min} = \sqrt{2} \times I_{PV\max} \quad (14)$$

where I_{PVmax} represents the highest PV string current.

IV. Control System Configuration

A. Current Controller

The configuration of the proposed current controller is presented in Fig. 2(a). The controller has two control loops: the inner current loop and the outer voltage loop. The voltage loop contains a PI controller to regulate the total voltage of the dc buses to the reference value $\sum V^*_{dc}$. Then, the output of the PI controller is multiplied by a unity sine-wave ($sin(\omega t+\varphi)$) to form the reference current i^*_s.

The initial phase (φ) controls the PF of the inverter.

The ac-side voltage of the inverter V^*_{AB} is calculated by the current controller. The current controller in this

configuration can be implemented using any desired scheme. This provides superior design flexibility to the control system.

B. DC Voltage Controller

The dc voltage controller scheme in this paper involves the use of two PI controllers to regulate the flowing current to each cell (see Fig. 2(b)).

The three cell utilization coefficients (CU_1, CU_2 and CU_3) are defined, where the APTC of the ac-side voltage is shared between the cells proportional to the corresponding coefficient, as follows:

$$(v^*_{Hj})_P=\frac{CU_j}{\sum_{k=1}^{3}CU_k}(v^*_{AB})_P \tag{15}$$

One of these coefficients (e.g. CU_3) is taken constant (e.g. unity) and the others are produced by two PI regulators, each of which takes the corresponding dc voltage error as the input.

Using this control scheme, since the overall dc voltage is controlled through the current controller and V_{dc1} and V_{dc2} are controlled through the corresponding coefficients, V_{dc3} is also automatically controlled.

C. Reactive power controller

The proposed reactive power controller keeps the PF of the inverter as close to unity as possible. To do so, in each sampling period the value of I_{sd} is calculated based on (8) and then compared to the minimum stable current of the inverter (according to (14)). If the value of I_{sd} is greater than I_{smin}, further action of the reactive power controller is disabled, the PF is kept at unity and no reactive power is exchanged with the grid.

If the value of I_{sd} is smaller than I_{smin}, according to (7), the inverter current should be increased to reduce the modulation index of the unstable cell. To do so, the inverter should absorb reactive power from or deliver reactive power to the grid which depends on the design preferences.

To stabilize the operation of the inverter with the highest possible PF, the conditions of (14) should be achieved. Thus the minimum phase shift (φ_{min}) which should be added to the reference current (according to Fig. 2) is derived as:

$$\varphi=\varphi_{\min}=-\tan^{-1}\left(\frac{\sqrt{I^2_{s\min}-I^2_{sd}}}{I_{sd}}\right) \tag{16}$$

Based on the reactive power balance, the ac-side voltage RPTC can be calculated as:

$$(V^*_{AB})_Q=\frac{E\times\sqrt{I^2_{s\min}-I^2_{sd}}}{I_{s\min}}=E\times\sin(\varphi) \tag{17}$$

After its calculation, the RPTC should be distributed between the cells with a lower PV current (lightly-loaded cells). This allocation can be performed in many ways, but the preferred way is to equalize the apparent power of the cells to evenly distribute the losses among them.

The capacity of each cell to produce the RPTC can be calculated as:

$$(V_{Hj})_{Q\max}=\sqrt{\left(\frac{V^*_{dcj}}{\sqrt{2}}\right)^2-(V_{Hj})^2_P} \tag{18}$$

where:

$$(V_{Hj})_P=\frac{P_j}{I_s} \tag{19}$$

To separate the active and reactive power transferring components and to share the RPTC between the lightly-loaded cells, this component is subtracted from the ac-side voltage reference of the inverter (the output of the current controller), after it is converted from phasor form to a real-time variable (by multiplication of its amplitude to a unity sine-wave with a $\varphi+\pi/2$ phase-shift). Then, the RPTC is divided between the lightly-loaded cells in such a way that the allocated portion to each cell does not exceed $(V_{Hj})_{Qmax}$ calculated by (18). The associated real-time signal of the allocated portions is then added to the reference voltage of each cell, as can be seen in Fig. 2(b).

The presented procedure is always valid for two cell inverters. However, for inverters with a higher number of cells, there may be an exception where the required RPTC can not be produced using the available capacity. This complication most likely arises when the inverter operates with a high modulation index and there are a few lightly-loaded cells. To solve this problem, the PF of the inverter should be further decreased to increase the input current of the inverter and to enhance the reactive voltage production capability of the inverter.

V. Simulation Results

The effectiveness of the CHB-based grid-connected PV inverter in Fig. 1 with a PR current controller [13] and the proposed voltage balancing and reactive power control methods have been evaluated based on digital time domain simulation studies in the PSCAD/EMTDC environment. The parameters of the experimental system are listed in Table I. Each CHB cell is connected to an array of three series-connected panels, whose parameters are listed in Table II. In this simulation, a 3mF capacitor is used as a smoothing capacitor in each cell to keep the dc voltage ripples below 8.5% [14] and the solar panel models are based on [15]. The Incremental Conductance (INC) method [16] is used for

TABLE I

PARAMETERS OF THE UNDER EXPERIMENT SYSTEM

Parameter	Value
Rated Grid Voltage	140 V
Inductor Filter	4 mH
Smoothing Capacitor	3 mF
Switching Frequency	3 kHz

TABLE II

PARAMETERS OF THE REC SOLAR 220AE PANELS

Parameter	Value
MPP voltage	28.7 V
MPP current	7.7 A
Open circuit voltage	36.6 V
Short circuit current	8.2 A
Temperature	25°C

MPPT which updates the reference voltages every Δt = .5s by ΔV = .5V. The simulations have been done with the initial conditions of G = 800 W/m^2 for the solar irradiation and T = 35°C for each PV array.

To evaluate the effectiveness of the proposed control scheme to follow the MPP, in the first simulation the temperature of the first array is changed from T_1 = 35°C to 25°C at t_1 = 9s, the temperature of the second array is changed from T_2 = 35°C to 45°C at t_2 = 12s, and the third array is changed from T_3 = 35°C to 25°C at t_3 = 14s. Fig. 3 illustrates the dynamic of the dc voltages, where the solid black lines represent the reference voltage of the dc links (generated by the MPPT) and the color waveforms demonstrate the voltage of the dc links (or the PV strings). In this study, the reference voltage of the dc links has been set to V_{refdc} = 85V at first. Then, the MPPT algorithm sets the reference voltage of the PV arrays close to the MPP point which is almost 83V for the initial test condition. To better compare the results, the reference voltages and the voltage of the dc links (after passing through a low-pass filter) have been illustrated in Fig. 4. An investigation of the results show that all of the dc links track rapidly and accurately their reference voltages. In addition, when the temperature of a cell decreases, the voltage of the corresponding cell increases and when the cell temperature increases, the corresponding cell voltage decrease in order to extract the maximum power from the connected PV array.

Fig. 5 illustrates the ac-side and grid voltage of the inverter. It can be seen that the CHB inverter generates a 7-level voltage waveform at the ac side and eliminates the need for large filters at the grid side. Finally, Fig. 6 demonstrates the rms voltage of the H-bride cells, i.e., V_{H1} to V_{H3}. It is evident that the proposed controller determines an appropriate modulation index for each cell to extract the maximum power from each PV array and to satisfy the power balance between the generated and the injected power.

The transferred active and reactive power of the cells during the first simulation are shown in Fig. 7. It can be seen that the generated power by the PV string has an inverse relation with the temperature. In addition, a small portion of the reactive power is transferred between the H-bridge cells and the grid due to presence of a filter inductor.

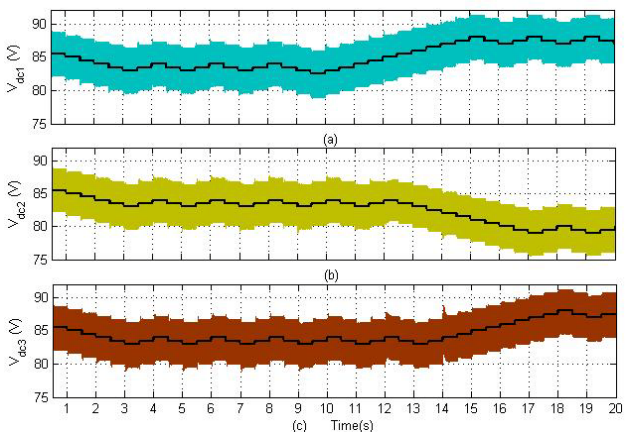

Fig. 3. Dynamic of the dc voltages during the first simulation: (a) Vdc1, (b) Vdc2, (c) Vdc3.

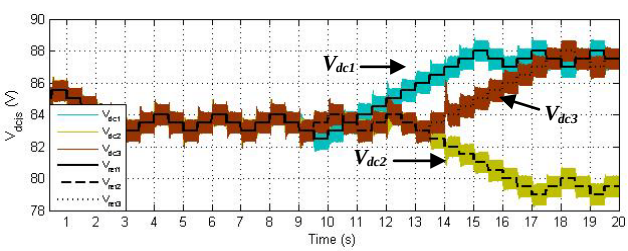

Fig. 4. Dc link voltages (after filtering) and corresponding reference values in the first simulation.

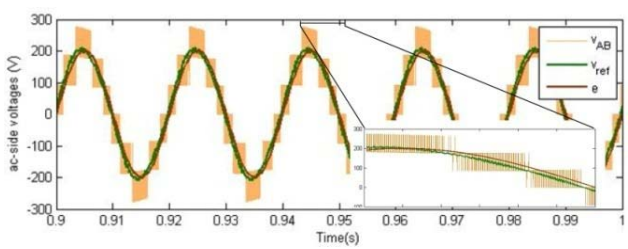

Fig. 5. Grid and ac-side voltage of the CHB inverter during the first simulation.

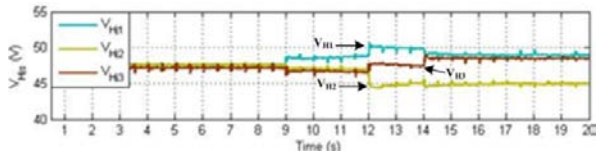

Fig. 6. The RMS voltage of H-bridge cells at the ac side during the first simulation.

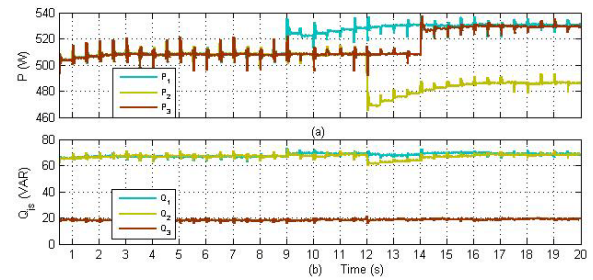

Fig. 7. Transferred active and reactive power of the cells during the first simulation: (a) transferred active power, (b) transferred reactive power.

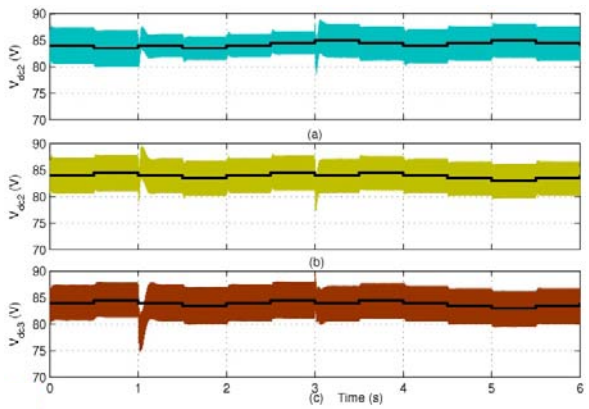

Fig. 8. Dynamic of the dc-bus voltages during a step change in irradiation of the first and second PV strings from 800 W/m2 to 500 and 200 W/m2.

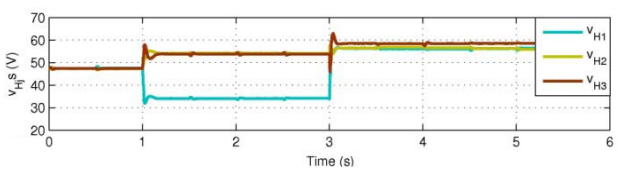

Fig. 9. The RMS of the ac-side voltage of the cells during the second simulation.

Another simulation has been carried out to assess the performance of the proposed reactive power controller under unbalanced PV conditions. After starting with the standard initial conditions, at t_1 = 1*s*, the irradiation level of the first PV array is changed from G_1 = 800 W/m^2 to 500 W/m^2. Then, at t_2 = 3*s*, a step change from G_2 = 800 W/m^2 to G_2 = 200 W/m^2 occurs in the irradiation level of the second PV array.

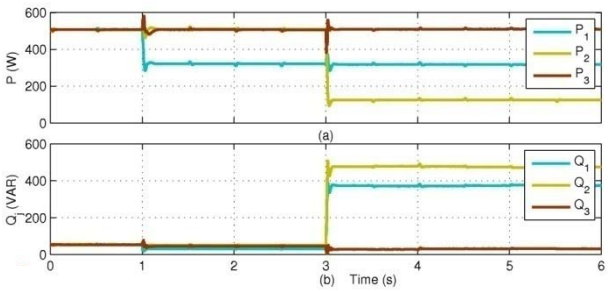

Fig. 10. Transferred active and reactive power of the cells during the second simulation: (a) transferred active power, (b) transferred reactive power.

As a result of the first change, the maximum power point current of the first PV array changes from I_{MPP1} = 6.18*A* to I_{MPP1} = 3.85*A*. Based on (11) the inverter is still stable under this condition when all modulation indices are smaller than unity and there is no need to exchange reactive power of the grid. However, after the second change and with I_{MPP2} = 1.52*A*, the stable operation of the inverter is not possible without the action of the reactive power controller.

The results of the second simulation are presented in Figs. 8-10. Fig. 8 shows the dynamics of the dc voltages during the second simulation and it demonstrates the ability of the proposed reactive power controller to maintain the stability of the converter. Fig. 9, shows the ac-side voltage of the cells. As can be seen the successful operation of the reactive power controller prevents the modulation index of the cells from exceeding unity. The transferred active and reactive power of the cells are also shown in Fig. 10.

VI. EXPERIMNTAL RESULTS

After the simulations, the validity of the proposed method is verified by using the experimental results from a 2000*W* laboratory prototype. The prototype is a single-phase, seven-level CHB inverter with three series-connected H-bridges at the ac side. Furthermore, the dc link of each H-bridge is connected to an array of three series-connected panels, whose parameters are listed in Table II. The other principal parameters of the prototype are given in Table III.

In the first experiment, the steady state behavior of the grid connected system is evaluated in the balanced condition. The employed MPPT algorithm (which is based on the INC method) will update the reference voltages every Δt = 1*s* by ΔV = 2*V*.

Fig. 11 demonstrates the voltage of the dc links at the steady state. In this experiment, the average voltage of each cell is around 80*V* and the maximum power is extracted from the PV strings. The proposed controller also provides a rapid and accurate tracking of the MPP for PV strings without an

TABLE III
EXPERIMENTAL PROTOTYPE SPECIFICATIONS

Rated grid voltage	140 V
Rated grid frequency	50 Hz
Number of H-bridges	3
Inverter rated power	2000 W
Filter Inductor	6 mH
dc capacitor	2 mF
Switching frequency	3000 Hz
Sampling frequency	6000 Hz

additional dc/dc converter. The elimination of three intermediate dc/dc converters and independent control of the PV strings improves the system efficiency when compared to the conventional systems.

Fig. 12 illustrates the grid voltage (e), the ac terminal voltage (V_{AB}), and the injected current to the grid when it delivers $1.3kW$ of active power to the grid. Here, the proportional resonant (PR) current control strategy with third and fifth harmonics compensation has been used to program the injected current to be sinusoidal. The resulting PF is close to 0.99 and the current THD is lower than 5% which satisfies the IEEE-519 constraints.

The second experiment investigates the behavior of the proposed reactive power controller under the unbalanced condition. In this experiment, part of the first PV string is shaded intentionally. Due to the unbalanced situation of the PV strings, the controller reduces the inverter power factor from PF = 0.99 to 0.84 (as can be seen in Fig. 13) to prevent possible instabilities. The measured grid side voltage is $63V$ for the first cell, $61V$ for the second cell, and $55V$ for the third cell, whereas the voltage of each PV string is close to $80V$.

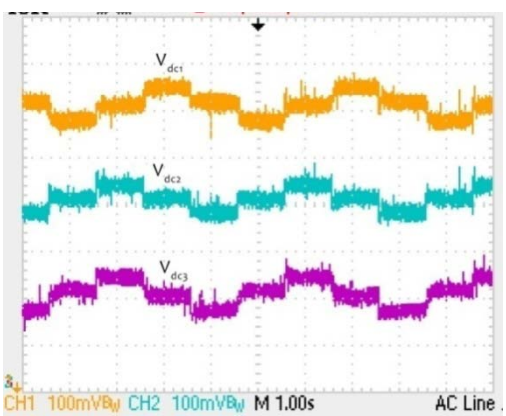

Fig. 11. Voltage of dc links during the first experiment (*v: 10V/div*).

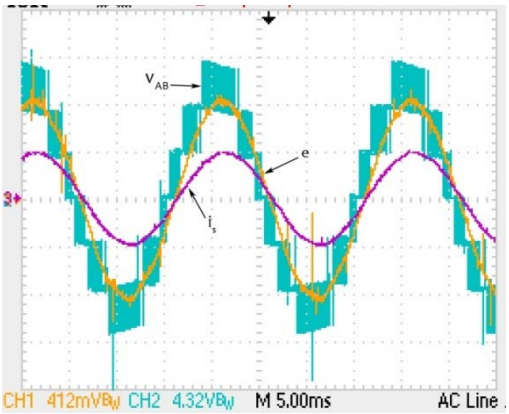

Fig. 12. Grid voltage (e), ac-side voltage (V_{AB}), and inverter current (i_s) during the balanced operating condition, *(i:15A/div, e:100V/div, v: 80V/div*).

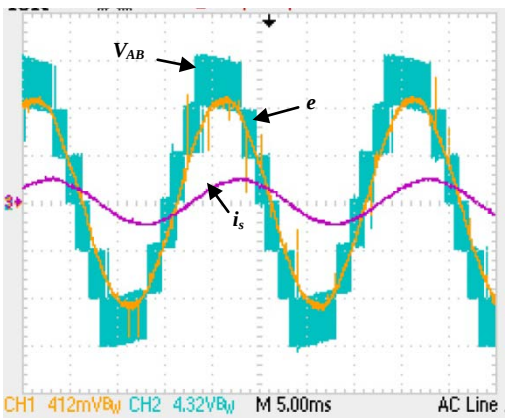

Fig. 13. Grid voltage, ac-side voltage, and inverter current during the imbalance operating condition, *(i:30A/div, e:100V/div, v: 80V/div*).

VII. CONCLUSIONS

This paper presents and evaluates a novel reactive power control strategy for CHB-based grid-connected PV systems. Based on the presented mathematical analysis, the proposed reactive power controller adjusts the inverter PF and manipulates the distribution of the reactive power between the cells to maintain the stability of the inverter. An appropriate voltage controller has also been proposed that enables fast and accurate tracking of the reference voltages.

The ability of the reactive power control strategy to stabilize the inverter operation, the performance of the proposed dc voltage controller, and the overall performance of the grid-connected PV system were investigated based on digital time-domain simulation studies in the PSCAD/EMTDC environment. The effectiveness of the proposed controllers were demonstrated under various PV and dc voltage conditions. The studies conclude that the

reactive power control strategy prevents the inverter system from becoming unstable under heavy unbalanced PV conditions.

REFERENCES

[1] S. B. Kjaer, J. K. Pedersen, and F. Blaabjerg, "A review of single-phase grid-connected inverters for photovoltaic modules," *IEEE Trans. Ind. Appl.*, Vol. 41, No. 5, pp. 1292-1306, Sep./Oct. 2005.

[2] J. Rodriguez, J. S. Lai, and F. Z. Peng, "Multilevel inverters: a survey of topologies, controls, and applications," *IEEE Trans. Ind. Electron.*, Vol. 49, No. 4, pp. 724–738, Aug. 2002.

[3] S. Daher, J. Schmid, and F. L. M. Antunes, "Multilevel inverter topologies for stand-alone pv systems," *IEEE Trans. Ind. Electron.*, Vol. 55, No. 7, pp. 2703-2712, Jul. 2008.

[4] L. G. Franquelo, J. Rodriguez, J. I. Leon, S. Kouro, R. Portillo, and M. A. M. Prats, "The age of multilevel converters arrives," *IEEE Ind. Electron. Mag.*, Vol. 2, No. 2, pp. 28-39, Jun. 2008.

[5] H. Imaneini, J. L. Schanen, S. Farhangi, and J. Roudet, "A modular strategy for control and voltage balancing of cascaded H-bridge rectifiers," *IEEE Trans. Power Electron.*, Vol. 23, No. 5, pp. 2428-2442, Sep. 2008.

[6] Dell'Aquila, M. Liserre, V. G. Monopoli, and P. Rotondoi, "Overview of PI-based solutions for the control of DC buses of a single-phase H-bridge multilevel active rectifier," *IEEE Trans. Ind. Appl.*, Vol. 44, No. 3, pp. 857-866, May/Jun. 2008.

[7] Cecati, F. Ciancetta, and P. Siano, "A multilevel inverter for photovoltaic systems with fuzzy logic control," *IEEE Trans. Ind. Electron.*, Vol. 57, No. 12, pp. 4115-4125, Dec. 2010.

[8] E. Villanueva, P. Correa, J. Rodriguez, and M. Pacas, "Control of a single-phase cascaded h-bridge multilevel inverter for grid-connected photovoltaic systems," *IEEE Trans. Ind. Electron.*, Vol. 56, No. 11, pp. 4399-4406, Nov. 2009.

[9] S. Khomfoi and C. Aimsaard, "A 5-level cascaded hybrid multilevel inverter for interfacing with renewable energy resources," *in Proc. Of 6th ECTI-CON*, pp. 284-287, 2009.

[10] L. M. Tolbert and F. Z. Peng, "Multilevel converters as a utility interface for renewable energy systems," *in Proc. of IEEE Power Engineering Society Summer Meeting*, pp. 1271–1274, Jul. 2000.

[11] M. Malinowski, K. Gopakumar, J. Rodriguez, and M. A. Perez, "A survey on cascaded multilevel inverters," *IEEE Trans. Ind. Electron.*, Vol. 57, No. 7, pp. 2197-2206, Jul. 2010.

[12] M. A. Rezaei, S. Farhangi, and H. Iman-Eini, "Extending the operating range of cascaded h-bridge based multilevel rectifier under unbalanced load conditions," *in Proc. of PECON 2010*, pp. 780-785, Nov. 2010.

[13] D. N. Zmood and D. G. Holmes, "Stationary frame current regulation of PWM inverters with zero steady-state error," *IEEE Trans. Power Electron.*, Vol. 18, No. 3, pp. 814-822, May 2003.

[14] S. B. Kjaer, J. K. Pedersen, and F. Blaabjerg, "Maximum photovoltaic power tracking: an algorithm for rapidly changing atmospheric conditions," *IEEE Trans Ind. Appl.*, Vol. 41, No. 5, pp. 1292-1306, Sep./Oct. 2005.

[15] M. G. Villalva, J. R. Gazoli, and E. R. Filho, "Comprehensive approach to modeling and simulation of photovoltaic arrays," *IEEE Trans. Power Electron.*, Vol. 24, No. 5, pp. 1198-1208, May 2009.

[16] K. H. Hussein, I. Muta, T. Hoshino, and M. Osakada, "Maximum photovoltaic power tracking: an algorithm for rapidly changing atmospheric conditions," Proc. IEE-Generation, Transmission and Distribution, Vol. 142, No. 1, pp. 59-64, Jan. 1995.

Mohammad-Ali Rezaei received his B.S. and M.S. in Electrical Engineering from the University of Tehran, Tehran, Iran, in 2008 and 2011, respectively. He is currently pursuing his Ph.D. in Electrical Engineering at North Carolina State University, Raleigh, North Carolina, USA. His current research interests include high power electronics and renewable energy grid integration systems.

Hossein Iman-Eini received his B.S. and M.S. from the University of Tehran, Tehran, Iran, in 2001 and 2003, respectively, and his Ph.D. from both the University of Tehran and the Grenoble Institute of Technology, France, in 2009, all in Electrical Engineering. He is currently an Assistant Professor in the School of Electrical and Computer Engineering, University of Tehran. His current research interests include the modeling and control of power converters, multilevel converters and renewable energy systems.

Shahrokh Farhangi received his B.S., M.S. and Ph.D. in Electrical Engineering from the University of Tehran, Tehran, Iran, with honors. He is a Professor in the School of Electrical and Computer Engineering, University of Tehran. His current research interests include the design and modeling of power electronic converters, drives, photovoltaic and renewable energy systems. He has published more than 90 papers in conference proceedings and journals.